Analytical Force Calculation in Brushless-DC Motors I: An Alternative Approach

Ewgenij Starschich
University of Warwick
Coventry, CV4 7AL, UK
e.starschich@warwick.ac.uk

Annette Muetze
University of Warwick
Coventry, CV4 7AL, UK
a.muetze@warwick.ac.uk

Kay Hameyer
RWTH Aachen University
52056 Aachen, Germany
kay.hameyer@iem.rwth-aachen.de

***Abstract*—In this paper, we focus on the analytical calculation of the tangential forces that generate the armature and the cogging torque in brushless dc machines. We extend previously presented methods using conformal mapping to (i) avoid the singularity of the magnetic flux density at the tooth tip during the transformation and thereby overcome the limitations of this approach with respect to the calculation of the cogging and armature torques developed in electric machines, and (ii) calculate the forces at the slot sides so that the influence of the machine design parameters on the result is directly available.**

***Index Terms*—Conformal mapping, brushless DC machine, design methodology, optimization.**

NOMENCLATURE

BLDCM	Brushless DC machine
EMF	Electromotive force
FEM	Finite element method
PM	PM
a	Transformation point in the conf. transf. $Z \rightarrow W$
b	Transformation point in the conf. transf. $Z \rightarrow W$
B	Magnetic flux density
d_s	Slot depth
f	Force density
f_v	Volumic force density
F_a	Armature force
F_c	Cogging force
g'	Air gap width in the Z-plane
H	Magnetic field strength
J	Current density
k	Coordinates in the K-plane
l_i	Effective machine length
p	Compressive stress tensor
R	Radius (machine geometry)
R_s	Stator inner surface radius
s	Coordinates in the S-plane
S^m	Maxwell stress tensor
t	Coordinates in the T-plane
w	Coordinates in the W-plane
ε	Auxiliary parameter
$\lambda_{ks,m}$	Coordinate transformation factor for $K \rightarrow S$ (calculation of the PM field)
$\lambda_{ts,a}$	Coordinate transformation factor for $T \rightarrow S$ (calculation of the armature winding field)
μ	Permeability
μ_0	Permeability of vacuum, $\mu_0 = 4\,\pi 10^{-7}$ Vs/(Am)
μ_{fe}	Permeability of iron
μ_r	Relative permeability
σ	Tensile stress tensor
σ	Auxiliary parameter
θ	Angle (machine geometry)

Indices

1	Parameter on slot side no. 1
2	Parameter on slot side no. 2
a	Parameter related to the armature winding field
m	Parameter related to the PM field
n	Component perpendicular to the material surface
t	Component tangential to the material surface

I. INTRODUCTION

In the light of an increasing complexity of electric drive systems development of efficient design techniques for electric machines that still meet the desired degree of accuracy are of high importance. In this paper, we focus on the analytical calculation of the tangential forces that generate the armature and the cogging torque in brushless dc machines (BLDCMs). We extend previously presented methods using conformal mapping to (i) avoid the singularity of the magnetic flux density at the tooth tip during the transformation and thereby overcome the limitations of this approach with respect to the calculation of the cogging and armature torques developed in electric machines, and (ii) calculate the forces at the slot sides so that the influence of the machine design parameters on the result is directly available.

We have chosen BLDCMs as our application for two reasons: (a) Because of the nonsinusoidal variation of the magnetic flux along the circumference, the armature torque of the BLDCM is calculated using the "original" abc-equations [1], [2]. (b) A wide range of motor- and controller-based design techniques have been developed to minimize the generation of cogging and ripple torques in BLDCM drives. These include the use of active cancellation algorithms which depend on either accurate tuning or adaptive control schemes [3], requiring a detailed analysis of the instant torque generation in BLDCM. Using an analytical technique that takes into account both the armature and the pulsating torque, the machine parameters can be optimized fast and together with the control technique in one step. Thereby, time-consuming, computationally expensive techniques such as the finite element method (FEM) only need to be used very selectively and towards the end of the design process.

We apply our technique to discuss the two macroscopical tangential forces occurring in electric machines, namely (a) the intended armature torque and (b) the parasitic cogging torque that results from the interaction of the magnets and the stator teeth. However, this should not obscure the fact that the presented technique can be expanded to be used in

different machines and for the calculation of radial forces which can cause deformation of stator and rotor iron, vibration and increased noise [4].

Seeking to convey the methodology itself and not to distract the reader through extensive discussion of long formulae and their derivations, we have split our contribution into two parts: the present Part I discusses the methodology of the new technique and Part II deals with the explicit derivation of the different formulae, where both parts are self-contained and can also be understood as stand-alone papers. In this paper, following a brief overview of the common methods to calculate magnetic forces in electric machines (Sec. II), we discuss the Maxwell stress theory (Sec. III), the analytical calculation of the magnetic forces and of the magnetic fields in the slots (Secs. IV and V), and apply these to calculate the armature and cogging torques in an example machine (Sec. VI), using the newly developed approach.

II. Overview of Methods to Calculate Magnetic Forces in Electric Machines

In the context of electric machines, four methods are commonly used to calculate the forces and torques [4]: the (i) Maxwell stress tensor, (ii) co-energy, (iii) rate of change of field energy, and (iv) the Lorentz force methods. The use of the *Maxwell stress tensor* requires the vectors of the flux density along a specific line or contour. The *co-energy* and *rate of change of field energy* methods do not require computation of the accurate distribution of the magnetic field itself, but at the expense that the force distribution inside the machine is not directly available. Because it is very easy to understand and does not require any further analysis of the physical background, the *Lorentz force* method is easy to apply and is therefore used in many books. Here, aiming to develop an analytical and fast design technique that comprises a direct correlation between the machine design and both the developed armature and cogging torque, we expand the Maxwell stress theory beyond its common use (i).

III. Discussion of the Maxwell Stress Theory

A. Introduction

The Maxwell stress theory can be used to calculate (A) the force on a rigid body placed in an electromagnetic field and (B) forces on the interface between materials with different permeabilities. While both approaches are suitable to calculate the torque in electric machines ((A): e.g. [5]–[6], [7]–[10]; (B): e.g. [11], [12].), only the force on a rigid body method, (A), is commonly used (mostly with FEM programs), and very few results using (B) exist. In our contribution, we focus on method (B), because of its suitability for analytical design and optimization techniques and the direct availability of the correlation between the machine geometrical parameters and the produced torque. For additional clarity, and to illustrate the difference between the two applications of the Maxwell stress theory, we also briefly review the expressions for use with method (A), before we discuss those occurring in the context of method (B). For a detailed analysis of the expressions, we refer to Part II.

B. Force on a rigid body placed in an electromagnetic field

The mutual forces between elements of charge are calculated via the assumption that a fictitious state of stress exists throughout the field, even in space free of matter, where the representation of magnetostatic stress components has no essential physical reality [13]. The force density f_m at the boundary of a given rigid body placed in an electromagnetic field is given by

$$\vec{S}^m \cdot \vec{n} = f_m = \frac{1}{\mu_0}\left(\vec{B}\cdot\vec{n}\right)\cdot\vec{B} - \frac{1}{2\mu_0}B^2\cdot\vec{n}\ . \tag{1}$$

Using this approach, the boundary of the region can be freely selected. In the context of electric machines, the contour is frequently placed in the air gap [14]. An advantage of this approach is that the contour can be selected in a way that singularities are avoided. However, the required calculation of not only the absolute values of the magnetic flux along this contour, but also of its vectorial components increases the computational complexity significantly. Furthermore, the relationship between the machine design parameters and the developed torque is not straightforward, since it is not obvious where the force physically occurs and therefore which part or parameter of the machine it is mostly influenced by.

C. Force on the interface between materials with different permeabilities

Maxwell was the first to give a mathematical expression to Faraday's concept of transmission of forces through a field, but his equations are almost certainly erroneous [12]. Helmholtz and Carter derived the formulations for calculation of the forces based on the energy stored in the magnetic material. Their derivations have the same concept, but differ in the material assumptions [12]. In both cases, the resulting force is directed from the area with higher to the one with lower permeability. No complete derivation of the forces between materials with different permeabilities could be found in available literature. In [11], the force direction is derived generally, but no material properties are taken into account. In [12], emphasis is placed on the material properties but the force components and their directions are not analyzed. In this paper, we combine these two approaches to calculate the force components into the different directions and taking the material properties into account.

The derivation of the forces between materials with different permeabilities is based on the assumption that a tensile stress σ exists inside a magnetic flux tube along the line of force trying to shorten the tube, and a compressive stress p at right angles to the line of force, trying to widen it [11]. Both σ and p depend on the material properties. In this paper, we shortly present both material assumptions and the resulting forces. For a detailed derivation of the latter, we refer to Part II of our contribution.

1) Helmholtz' material assumptions: The tensile and compressive forces σ and p, derived from Helmholtz' material assumptions, are [12]

$$\sigma = p = \frac{1}{2}BH\ , \tag{2}$$

The resulting forces acting at the interface between the materials are then

$$f_n = \frac{1}{2} \cdot \left(\frac{1}{\mu_1} - \frac{1}{\mu_2} \right) \left(B_{1n}^2 + \frac{\mu_2}{\mu_1} B_{1t}^2 \right) , \quad (3)$$

$$f_t = 0 . \quad (4)$$

With Helmholtz' material assumptions, the total force has only a normal force component. *The direct implication from the Helmholtz σ and p definitions for electric machine applications is that the torque can only be generated at the tooth sides. The field component at the tooth head causes radial forces and does not have a tangential force component*.

In the context discussed here, only the interfaces between iron and materials with $\mu \ll \mu_{fe}$ are of interest. Assuming $\mu_2 = \mu_r \mu_0$, $\mu_1 = \mu_0$ (Without loss of generality, we simplify $\mu = \mu_0$ throughout the whole slot.), and $\mu_r \to \infty$, (3) becomes finally

$$f_n = \frac{1}{2\mu_0} B^2 . \quad (5)$$

2) Carter's material assumptions: Carter made different material assumptions, resulting in [12]

$$\sigma = \frac{1}{2\mu_0} B^2 \quad \text{and} \quad p = \frac{\mu_0}{2} H^2 \quad (6)$$

for the tensile and compressive stresses, from which the normal and tangential force densities at the interface between two materials with $\mu_1 = \mu_0$ and $\mu_2 = \mu_r \mu_0$,

$$f_n = \frac{1}{2} \frac{B_{1n}^2 - H_{1t}^2}{\mu_0} - \frac{1}{2} \left(\frac{B_{2n}^2}{\mu_0} - \mu_0 H_{2t}^2 \right) = 0 , \quad (7)$$

$$f_t = -\frac{(\mu_r - 1)^2}{2\mu_r} \cdot H_{1n} \cdot H_{1t} \quad (8)$$

are obtained.

Using Carter's material assumptions, only a tangential force exists at the interface between materials with different permeabilites. However, as the magnetic field becomes perpendicular to the surface for $\mu_r \to \infty$, the tangential force component (8) would also diminish for this "ideal" case.

Unlike with Helmholtz' assumptions, Carter's material assumptions and therefrom derived stresses can also cause forces within the material. The volumic iron force density inside the material is given by

$$f_v = \vec{J} \times \vec{B} + \mu_0 \left(\frac{\mu_r^2 - 1}{2} \right) \nabla \left(\frac{1}{2} H^2 \right) , \quad (9)$$

where the term $\vec{J} \times \vec{B}$ expresses a force density due to currents within the iron, which–neglecting eddy currents–are usually not present. The second term gives the force density which is directed towards the regions with a higher flux density.

D. Conclusions on the material assumptions

The two different definitions of σ and p lead to significantly different results of the developed forces which (for μ_1 and μ_2 as defined above) can be summarized as follows:

1) Helmholtz' material assumptions give surface forces normal to the surface, but no volumic forces. The surface forces do not depend on the orientation of the flux but only on its absolute magnitude, and are directed from the material with the higher to the one with the lower permeability.
2) Carter's material assumptions give both surface and volumic forces. The surface forces are tangential to the surface and are zero when the magnetic field is tangential or perpendicular to the surface. The volumic forces inside the material tend to force each element towards the parts with the higher magnetic flux density.

For accurate analysis of the forces acting inside a machine, both assumptions should be examined. However, the authors are not aware of any literature in which Carter's material assumptions are used and the machine torque is analyzed based on the field calculated inside the iron. *In the further analysis, Helmholtz' material assumptions will be used* because the resulting analysis is more concordant with the common techniques of machine analysis and the calculation of the field inside the iron of the machine is more complex than the one at the material interfaces.

IV. Calculation of the magnetic forces

A. Cogging force

The cogging torque is caused by the tendency of the rotor to align with the stator slots in such a position that the total permeance of the magnetic circuit seen by the permanent magnets (PMs) is maximized [15]. Considering Fig. 1(a), the magnetic flux from the magnet to sides 1 and 4 and to sides 2 and 3 and hence the forces at the material interfaces are equal,

$$|\vec{F}_{c1}| = |\vec{F}_{c4}| \quad \text{and} \quad |\vec{F}_{c2}| = |\vec{F}_{c3}| , \quad (10)$$

thus cancel each other, and no force acts upon the rotor. A displacement of the stator with respect to the rotor causes a change of the flux entering the four slot sides and thus of the four forces $\vec{F}_{c1}$ to $\vec{F}_{c4}$. In Fig. 1(b)), $\vec{F}_{c3}$ and $\vec{F}_{c4}$ have increased and $\vec{F}_{c1}$ and $\vec{F}_{c2}$ decreased. As long as the flux density entering sides 1 and 3 is higher than the one entering sides 2 and 4, the forces $\vec{F}_{c1}$ and $\vec{F}_{c3}$ pull the stator back to the previous position. When the flux density entering sides 1 and 3 becomes smaller, the direction of the overall force changes. Since the flux and therefore the forces on the two tooth sides of a slot completely covered by a magnet are equal, *cogging torque can only be produced in those slots that are partially covered by magnets*.

Using the force density as given by (5), the total force acting on one slot side is

$$F_c = \frac{1}{2\mu_0} \cdot l_i \cdot \int_{R_s}^{R_s + d_s} B_m^2 \, dR . \quad (11)$$

In contrast to the calculation of the cogging torque using the force on a rigid body/contour in the air gap method, *only the absolute value of the flux distribution along the slot sides is required here*.

B. Armature force

Here, unlike in the case of the cogging torque, the difference of the forces acting on the two slot sides is caused by the armature winding field, since a part of the magnetic flux

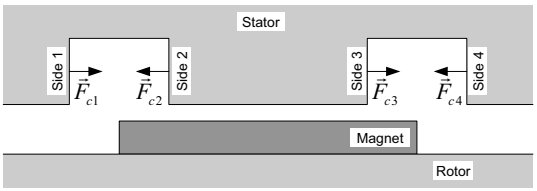

(a) Position in which the PM covers $1/2$ of the left and $1/2$ of the right slot respectively.

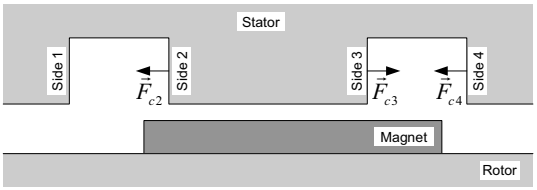

(b) Position in which the PM covers $1/4$ of the left and $3/4$ of the right slot respectively. In this position, F_{c1} becomes negligible small.

Fig. 1. Magnet positions and generation of cogging torque.

created by the winding leaves the slot on one side and enters on the other side again (Fig. 2(a)). Overlapping the armature and the PM (Fig. 2(b)) fields illustrates that the latter is weakened on side 1 and increased on side 2.

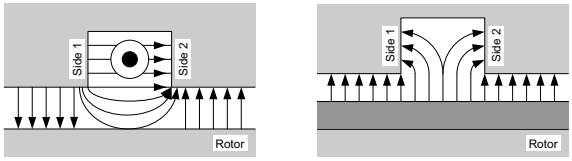

(a) Armature winding flux. (b) PM flux.

Fig. 2. Magnetic flux generated by armature winding current and PMs.

Considering that $\vec{B}_m || \vec{B}_a$ at θ_1 and θ_2 (sides 1 and 2) and whether the two fields are oriented into the same or into the opposite direction, the resulting force in the slot is derived using (11),

$$F_a = \frac{1}{2\mu_0} \cdot l_i \cdot \int_{R_s}^{R_s+d_s} \left(\left| \vec{B}_m(R,\theta_2) - \vec{B}_a(R,\theta_2) \right|^2 - \left| \vec{B}_m(R,\theta_1) + \vec{B}_a(R,\theta_1) \right|^2 \right) dR \,. \quad (12)$$

With $|\vec{B}(R,\theta_1)| = |\vec{B}(R,\theta_2)| = |\vec{B}(R)|$, both for B_m and B_a, we obtain

$$F_a = -\frac{2}{\mu_0} \cdot l_i \cdot \int_{R_s}^{R_s+d_s} \left| \vec{B}_m(R) \right| \left| \vec{B}_a(R) \right| \, dR \,. \quad (13)$$

Again, *only the absolute values of the fluxes generated by the PMs and by the armature winding, but not their normal and tangential components, need to be determined.*

V. Analytical Calculation of the Magnetic Field in the Slots

A. Introduction

Conventionally, in contexts where the magnetic resistance of the air gap is calculated, the slot openings are taken into account via the Carter factor (e.g. [16], [17]). However, this approach precludes information on the radial and tangential components as well as an accurate calculation of the magnetic flux on the slot sides, as it is required for the approach to calculate the tangential forces developed in the machine discussed here.

In [7], [9] and [18], [19] respectively, the magnetic field, including the one in the slot, is calculated in two steps: First, the air gap field is calculated for a slotless machine (Fig. 3) and then the slotting is taken into account through multiplication with a complex permeance. The methods presented subsequently in [7], [9] and [18], [19] differ with respect to the approaches taken to calculate the magnetic field and the permeance: In [18], the field is calculated by modeling the PM with a current distribution in the air gap and the effect of the stator slotting is then considered in [19] by assuming the flux density under the slot to be zero and the entire flux over the slot pitch entering the stator under the tooth. Since this assumption contradicts the technique used here ($B_{n,\text{slotsides}} = 0$ and hence $F_a = F_c = 0$), it is not discussed and/or developed any further.

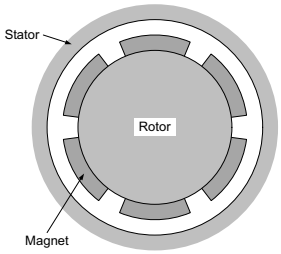

Fig. 3. Slotless PM machine.

In [7], the air gap flux density generated by the PMs in a slottless machine is calculated by solving the Poisson equation. In [9], the effect of slotting is implemented using conformal mapping, and in [8] the approach is adapted to calculate the armature winding field. Assuming the two fields can be calculated independently from each other, the overall air gap field is then obtained through superposition in [10]. Because of the different distributions of the PMs and of the armature winding, two different conformal mappings are required to calculate the flux generated from these two sources respectively.

The following simplifications are made: (i) $\mu_{fe} \rightarrow \infty$, (ii) no change of the field distribution in axial direction, (iii) rectangular, and (iv) infinitely deep slots, where the last two simplifications are required for the conformal mapping. It will be shown below, that (iv) does not have any significant influence on the force calculation (Sec. VI).

In this work, we use the conformal transformation used in [20] for the calculation of the magnetic field generated by the armature winding and the one presented in [5] (which is based on [7], [9], and [20]) for the computation of the field generated by the PMs, respectively. (Note again that [18] and [19] use a slightly different approach.) For the derivation of the magnetic field distributions in a slotless PM machine and of the complex permeances λ_m^* and λ_a^* we refer to the literature (i.e. [5], [20]) and only summarize the key aspects and equations that we then used in the following.

B. Magnetic field distribution in a slotless PM machine

The PMs are (i) assumed to have a linear second-quadrant demagnetization characteristic, (ii) are modeled by surface currents at the magnet flanks, neglecting any volume currents inside the PMs [18], and (iii) are radially magnetized (see also simplification (ii) in Sec. V-A). In our context, only the magnetic flux density in the area covered by air is of interest. For the derivation as well as the explicit equation this magnetic flux density, we refer to [7].

C. Conformal transformation of the PM field

Four conformal transformations are required for the determination of the magnetic field in the machine slots, transforming the geometry between the planes S, Z, W, T and K [5] (Fig. 4). In the first transformation, the circular machine shape given in the S-plane is transformed into a linear model in the Z-plane using a logarithmic conformal transformation ($S \rightarrow Z$). Then, the polygon boundaries of the Z-plane are transformed into the upper half of the W-plane with the Schwarz-Christoffel transformation ($Z \rightarrow W$). Note that, per its definition, the Schwarz-Christoffel transformation realizes only the inverse transformation $W \rightarrow Z$. An analytic transformation $Z \rightarrow W$ is not possible and numerical methods have to be applied. Nevertheless, for simplicity, we adopt this name here. Note also that this transformation includes the determination of several integration parameters and constants. Next, the polygon in the W-plane is transformed into another polygonal form in the T-plane, again, using a Schwarz-Christoffel transformation ($W \rightarrow T$). In the last step, the original polygonal shape of the original S-plane is transformed into a circular slotless machine shape in the K-plane (Fig. 3) ($T \rightarrow K$) where the distribution of the magnetic field is known, using an exponential transformation.

Knowing the field in one plane and knowing also the conformal transformations between the planes it can be shown that [5], [21]

$$\vec{B}_{Plane\,A} = \vec{B}_{Plane\,B} \cdot \left(\frac{\partial Plane\,B}{\partial\, Plane\,A} \right)^* , \tag{14}$$

where '*' denotes the complex conjugate. Hence, the field in the slotted machine (S-plane) can be obtained from the one computed for the slotless machine (K-plane) using

$$B_{sm} = B_{km} \cdot \left(\frac{\partial k_m}{\partial s_m} \right)^* , \tag{15}$$

from which

$$B_{sm} = \lambda^*_{ks,m} \cdot B_{km} \tag{16}$$

with

$$\lambda_{ks,m} = \frac{k_m}{s_m} \cdot \frac{w_m - 1}{\sqrt{w_m - a_m}\sqrt{w_m - b_m}} = \lambda_m \tag{17}$$

is obtained. (Here, k, w, and s are the coordinates in the K-, W-, and S-plane respectively, $a_m = 1/b_m$ are transformation points for the transformation $Z \rightarrow W$, and the index m indicates that the magnetic field is generated by the PMs. Note that z and t do not appear in (17) because they can be expressed in terms of w.) It is important to note that (17) does not have a solution for $w_m = a_m = b_m$ which correspond to the tooth tips in the S-plane.

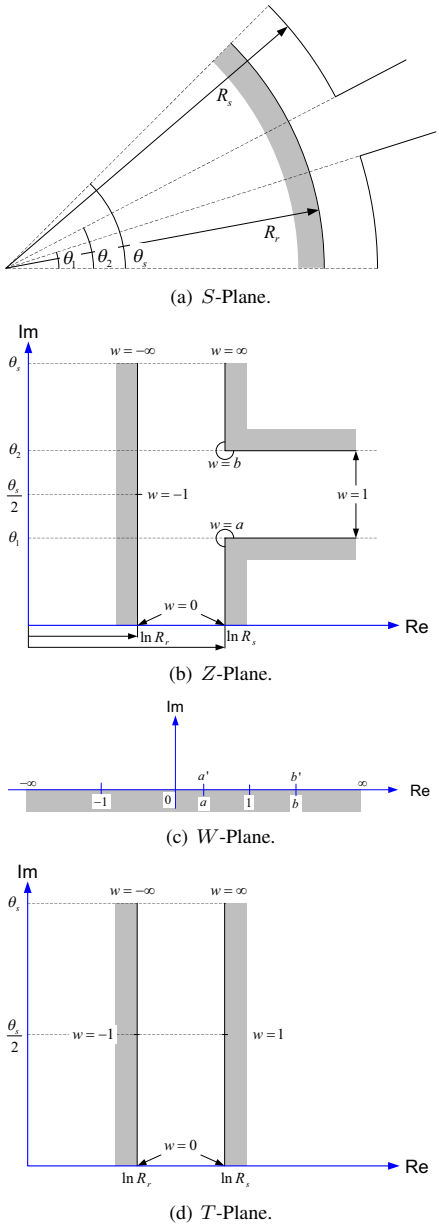

(a) S-Plane.

(b) Z-Plane.

(c) W-Plane.

(d) T-Plane.

Fig. 4. Conformal transformations for PM field.

D. Conformal transformation of the armature field

For the armature field, only three conformal transformations are required: $S \rightarrow Z$, $Z \rightarrow W$, and $W \rightarrow T$ (Fig. 5) [20]. Because of the usually small air gaps, the computations are restricted to only one infinitely deep slot with a current of $2I$ at its 'bottom,' and hence potentials of I and $-I$ at the two slot sides (with respect to the rotor at zero potential). Exploiting the line of symmetry [20] in the middle of the slot, only half of a slot needs to be analyzed.

Similar to above, the field in the slotted machine (S-plane) can be obtained from the one computed for the slotless machine (T-plane) using

$$B_{sa} = B_{ta} \cdot \left(\frac{\partial t_a}{\partial s_a} \right)^* , \tag{18}$$

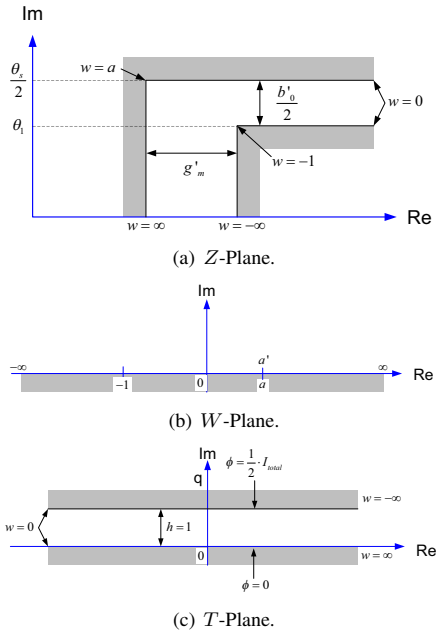

(a) Z-Plane.

(b) W-Plane.

(c) T-Plane.

Fig. 5. Conformal transformations for armature field.

from which

$$B_{sa} = \lambda^*_{ts,a} \cdot B_{ta} \tag{19}$$

with

$$\lambda_{ts,a} = j \cdot \frac{1}{g'} \frac{\sqrt{w_a - a_a}}{\sqrt{w_a + 1}} \cdot \frac{1}{s_a} = \lambda_a \tag{20}$$

is obtained. (Similar to above, w and s are the coordinates in the W- and S-plane respectively, a_a is a transformation point for the transformation $Z \rightarrow W$, the index a indicates that the magnetic field is generated by the armature winding, and g' denotes the width of the air gap in the Z-plane.)

VI. Force and Torque Calculations

A. Introduction

The magnetic forces F_c and F_a can be calculated (a) either in two consecutive steps, where first B_m and B_a are determined through conformal mapping and the results are then used to calculate F_c and F_a, (b) or in one step, where B_m and B_a in the expressions for F_c and F_a are replaced by their expressions including the conformal mapping factors λ^*_m and λ^*_a and the fluxes in the slotless machines B_{km} and B_{ta}. Thereby, only the forces F_c and F_a are calculated explicitly and in one step. Because of a singularity occurring at the tooth tip during the conformal mapping (see eqs. (17) and (20)), the application of the first approach is very limited: Since the flux density at the tooth tips cannot be determined, the integration boundaries are adjusted introducing an auxiliary parameter ε and the magnetic flux is only determined starting from at the distance ε from the tooth tip. Furthermore, to consider the finite depth of the slots in electric machines, a second auxiliary parameter σ is introduced and the magnetic field only determined by the length σ into the slot.

TABLE I
Parameters of the fictive machine.

Magnet remanence flux density	1.3 T	Pole pairs	2
Relative recoil permeability	1.045	Slot depth d_s	10 mm
Magnet pitch ratio	2/3	Slot parameter θ_1	4°_{mech}
Radius rotor surface	55 mm	Slot parameter θ_2	6°_{mech}
Radius magnet surface	57 mm	Slot parameter θ_s	10°_{mech}
Radius inner stator surface (R_s)	57.5 mm		

The outcomes of the computations are very sensitive to the value of the parameter ε (Sec. VI-B). With the second approach, this limitation can be overcome, and the method proves correct (Sec. VI-C). The calculations carried out in the following are based on a fictive machine (Table I).

B. Force and torque calculations in two consecutive steps

The flux density at the slot side generated by the PMs is calculated using (16), using the auxiliary parameters ε and σ. These parameters are selected empirically, and a technique for correct determination could be a topic of further research. While σ does not have a crucial influence on the force calculation, ε has: approaching singularity at the tooth tip, a small change in ε has a huge influence on the flux density and therefore the force developed near the tooth tip. For the analysis, $\sigma = 4\,\text{mm}$ and two values of ε, $\varepsilon = 0.01\,\text{mm}$ and $\varepsilon = 0.007\,\text{mm}$ are chosen. The influence of the value of ε on the results is analyzed at the end of this section and $\varepsilon = 0.01\,\text{mm}$ is used in all other cases.

Two situations of the field generated by the PM have to be distinguished: (a) The slot opening is fully and (b) partially covered by a magnet: Fig. 6 shows the computed results for the first case, (a): although the slot depth is 10 mm, the flux density at the slot side is nearly zero after 3 mm and hence *the assumption of the infinite slot depth can be used without any restrictions because the force acts only at a fractional part of the slot side*. In the second case, (b), the flux densities and therefore the magnetic forces acting on the two slot sides are different, causing the cogging torque. The flux density in the slotless machine (K-plane) is no longer constant as in the first case (a) (Fig. 7). The width of the transition area depends on the geometrical parameters of the machine and notably on the dimensions of the magnet.

The field on the slot sides created by the armature winding is calculated using (19) and again the auxiliary parameters ε and σ. As can be seen from Fig. 8, the flux density does not decrease as strongly with the slot depth as in the previous case of the field generated by the PMs. However, it stays almost constant after 1.5 mm into the slot.

For the analytical torque calculation we only consider the forces acting on the slot side up to 3 mm into the slot. We set the radius at which the resultant force is active 1.5 mm into the slot, thereby introducing a maximum error of 3%. We also compare the results with those computed numerically by means of a commercially available FEM program. The results (Fig. 9) show that *the small difference of 0.003 mm for ε leads to a significant difference of the computed values*, where the torque increases with decreasing value of ε as expected: because of its dependency on the auxiliary parameter ε and the extreme sensitivity of the computed values on the

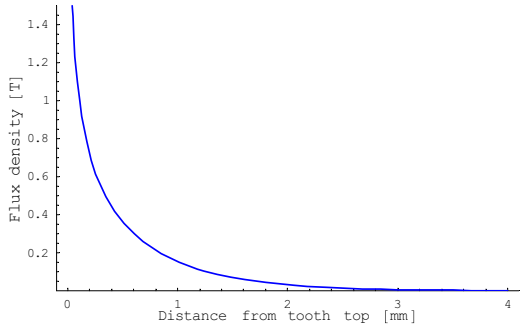

Fig. 6. Permanent magnet magnetic flux density at the slot side, computed 0.01 mm from the tooth tip 4 mm into the slot (corresponding to the auxiliary parameters $\varepsilon = 0.01$ mm and $\sigma = 4$ mm).

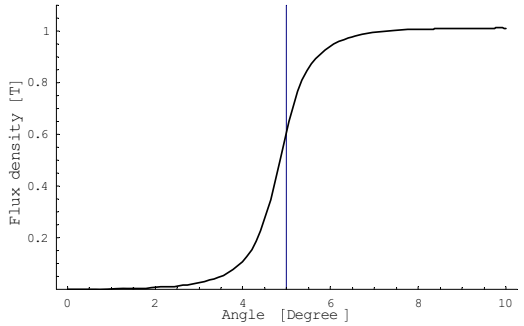

Fig. 7. Magnetic flux density at the inner stator surface in the slotless machine (K-plane) with the magnet edge in the middle of the slot (5°) in the slotted machine (S-plane).

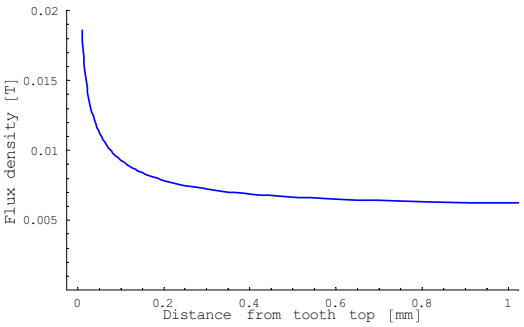

Fig. 8. Armature winding flux density at the slot side, computed as of 0.01 mm from the tooth tip (corresponding to the auxiliary parameter $\varepsilon = 0.01$ mm).

choice of ε, these values illustrate the limitations of this two-step approach. Therefore, calculation of the armature torque based on explicit computation of B_c and B_a does not add much value and is omitted. Before continuing with the second newly developed one-step approach, where B_c and B_a are not calculated explicitly, we note that the magnitude of the numerically computed torque is in-between the two analytically computed values. Furthermore, the numerical and analytical results are not in phase, indicating that the calculated flux densities do not reach their maxima at the same rotor displacements.

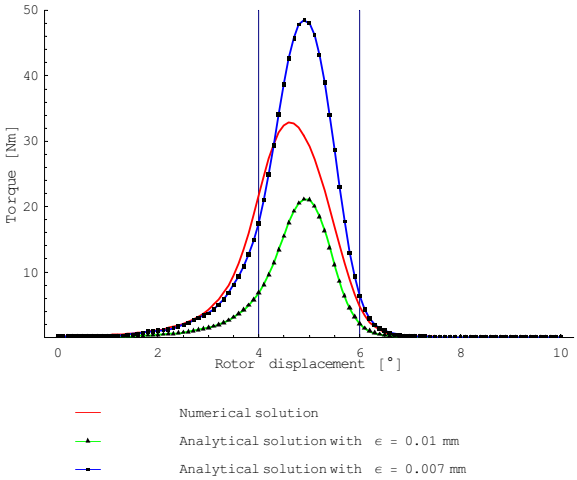

Fig. 9. Cogging torque calculated analytically for $\sigma = 4$ mm and $\varepsilon = 0.01$ mm as well as $\varepsilon = 0.007$ mm and numerically (FEM).

C. Force and torque calculations without explicit calculation of the magnetic flux density

1) Cogging torque: Substituting $B_m = B_{sm}$ in (11) with $\lambda^*_{ks,m} \cdot B_{km}$ according to (16) and adjusting the integration parameters, a new expression for the force acting on one given slot side is obtained,

$$F_c = \frac{1}{2\mu_0} \cdot l_i \cdot R_s \cdot \frac{g'}{\pi} \cdot \int \left\{ |B_{km}(w_m)|^2 \cdot \frac{1 - w_m}{w_m \cdot \sqrt{w_m - a_m} \cdot \sqrt{b_m - w_m}} \right\} dw_m \,, \quad (21)$$

where the integration limits are a and 1 on the first, and 1 and b on the second slot side. For the detailed derivation of (21) and of the integration limits, we refer to Part II of this paper.

We calculate the cogging torque based on the field in the slotless machine, $B_{km}(w)$, calculated both analytically (Sec. V-B) and numerically (FEM) and compare the results to the cogging torque calculated using FEM only (Fig. 10).

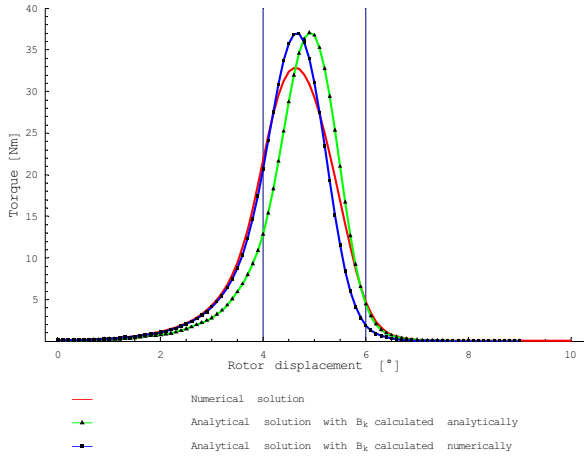

Fig. 10. Cogging torque calculated analytically according to (21), using the air gap field in the slotless machine computed analytically as well as numerically (FEM), compared to the numerically computed cogging torque.

The results confirm that *the new approach to compute the cogging torque based on the magnetic field in the slotless machine and using a single expression is justified*. However, since the purely analytical solution is again displaced when compared to the other two solutions, we conclude that the analytical calculation of the magnetic flux density in the slotless machine (Sec. V-B) leads to reasonable results for the torque magnitude but not for the position the maximum of the torque occurs at. Hence, further work to develop improved methods to calculate this field analytically would be preferable. However, *considering the sensitivity of numerical results for the cogging torque towards the simulation parameters and the related and required high computational effort, the results of the analytical calculation can be considered as acceptable.*

2) Armature torque: Similar to above, we substitute $B_a = B_{sa}$ in (13) with $\lambda^*_{ts,a} \cdot B_{ta}$ according to (19) and adjust the integration parameters to obtain a new expression for the force acting on one given slot side,

$$F_a = -\frac{2}{\mu_0 \pi} \cdot l_i \cdot |B_{km}| \cdot |B_{ta}| \cdot \int_{a_m}^{1} \frac{1}{w_m} \left| \frac{\sqrt{w_a(w_m) - a_a}}{\sqrt{w_a(w_m) + 1}} \right| dw_m \,. \quad (22)$$

Again, we refer to Part II for the explicit derivation of (22) and the adjusted integration limits.

Note that (22) cannot be solved analytically because of the numerical determination of the armature winding field W-plane variable w_a as a function of the PM field W-plane variable w_m, $w_a(w_m)$. This numerical determination is more complex than the one used to calculate the flux density only. However, *this new approach bypasses the singularity problem at the tooth tip, so that the force can be calculated without any restrictions.*

In the fictions machine, for simplicity, every pole has only one coil with one turn, carrying $10\,\mathrm{A}$, and is completely covered by the magnet. The rotor is placed in such a position that the magnet edges are not located at any slot opening to avoid cogging forces. The difference between the analytical and the numerical solutions is *smaller than* 1%*, which is an excellent result*. (Torque calculated using (22): $2.362\,\mathrm{Nm}$, torque calculated numerically (FEM): $2.363\,\mathrm{Nm}$.) It is likely that such accuracy will not be obtained for other machine configurations. *However, the results prove that the armature force calculation assumptions and the implementation of the conformal mapping into the calculation of the force are correct and that they generally can be used for the force calculation.*

VII. Conclusions

A comprehensive analysis of the use of the Maxwell stress theory applied to calculate the forces at the interface of two materials with different permeabilities (as opposed to the forces on a rigid body placed in an electromagnetic field) and thereby to compute the armature and cogging torque in BLDCMs was carried out. To this aim, the magnetic flux density at the slot sides is required. This was computed using available techniques to calculate the flux in slotted machines based on conformal transformations. Because of a singularity occurring at the tooth tip, and the crucial influence on the flux density in this area on the calculated torque, calculation of the torque based on flux densities determined via this method is very limited. To avoid the need to explicitly calculate the magnetic flux at the tooth tips, an alternative approach was taken, whereby the value of the flux density in the slotted machine was replaced by the value in the slotless machine and the corresponding transformation parameters. This method allows to calculate the tangential forces and hence the armature and the cogging torque without the restriction of not being able to properly consider the contribution of the tooth tip. The analytical calculation results of the armature force correlate very well with those obtained numerically.

References

[1] P. Pillay and R. Krishnan, "Modeling of permanent magnet motor drives," *IEEE Tr. Ind. Electr.*, vol. 35, no. 4, pp. 537–541, Nov 1988.

[2] P. Pillay and R. Krishnan, "Modeling, simulation, and analysis of permanent-magnet motordrives, Part II: The brushless DC motor drive," *IEEE Tr. Ind. Electr.*, vol. 25, no. 2, pp. 274–279, Mar/Apr 1989.

[3] T.M. Jahns and W.L. Soong, "Pulsating torque minimization techniques for permanent magnet AC motor drives-a review,", *IEEE Tr. Ind. Electr.*, vol. 43, no. 2, pp. 321–330, Apr 1996.

[4] J.F. Gieras and M. Wing, *Permanent magnet motor technology*, CRC Press, London, 2002.

[5] D. Zarko, D. Ban, and T.A. Lipo, "Analytical calculation of magnetic field distribution in the slotted air gap of a surface permanent-magnet motor using complex relative air-gap permeance," *IEEE Tr. Magnetics*, vol. 42, no. 7, pp. 1828–1837, Jul 2006.

[6] D. Zarko, D. Ban, and T.A. Lipo, "Analytical Solution for Cogging Torque in Surface Permanent-Magnet Motors Using Conformal Mapping," *IEEE Tr. Magnetics*, vol. 44, no. 1, pp. 52–65, Jan 2008.

[7] Z.Q. Zhu and D. Howe, "Instantaneous magnetic field distribution in brushless permanent magnet DC motors I: Open-circuit field," *IEEE Tr. Magnetics*, vol. 29, no. 1, pp. 124–135, Jan 1993.

[8] Z.Q. Zhu and D. Howe, "Instantaneous magnetic field distribution in brushless permanent magnet DC motors II: Armature-reaction field," *IEEE Tr. Magnetics*, vol. 29, no. 1, pp. 136–142, Jan 1993.

[9] Z.Q. Zhu and D. Howe, "Instantaneous magnetic field distribution in brushless permanent magnet DC motors III: Effect of stator slotting," *IEEE Tr. Magnetics*, vol. 29, no. 1, pp. 143–151, Jan 1993.

[10] Z.Q. Zhu and D. Howe, "Instantaneous magnetic field distribution in brushless permanent magnet DC motors IV: Magnetic field on load," *IEEE Tr. Magnetics*, vol. 29, no. 1, pp. 152–158, Jan 1993.

[11] K. Vogt and G. Mueller, *Berechnung rotierender elektrischer Maschinen*, VEB Verlag Technik Berlin, 1974.

[12] G.W. Carter, *The electromagnetic field in its engineering aspects*, Longman Group Limited, London, 1967.

[13] J.A. Stratton, *Electromagnetic theory*, McGraw-Hill, New York, London, 1941.

[14] W.R. Canders, "Grundlagen der Elektrischen Energietechnik-Elektrische Energieumformung," IMAB TU Braunschweig, Technical Report, 2007.

[15] T.J.E. Miller, *Brushless permanent-magnet and reluctance motor drives*, Clarendon Oxford, 1989.

[16] F.W. Carter, "Air-gap induction," *Electrical world and engineer* vol. XXXVIII, pp. 884–888, 1901.

[17] G. Müller, K. Vogt, and B. Ponick, *Berechnung elektrischer Maschinen* Series Elektrische Maschinen, vol. 2, 664 pages, Wiley-VCH, Berlin, 2007.

[18] N. Boules, "Prediction of No-Load Flux Density Distribution in Permanent Magnet Machines," *IEEE Tr. Ind. Appl.*, vol. IA-21, no. 3, pp. 633–643, May 1985.

[19] N. Boules and J. De La Ree, "Torque production in permanent-magnet synchronous motors," *IEEE Tr. Ind. Appl.*, vol. 25, no. 1, pp. 107–112, Jan/Feb 1989.

[20] K.J. Binns, P.J. Lawrenson, and C.W. Trowbridge, *The analytical and numerical solution of electric and magnetic fields*, John Wiley & Sons, Chichester, 1992.

[21] W.J. Gibbs, *Conformal Transformations in Electrical Engineering*, Chapman & Hall LTD, London, 1958.